The high resolution synchrotron-based imaging stations at the BAM*line* (BESSY) and TopoTomo (ANKA)

Alexander Rack*[a], Heinrich Riesemeier[b], Simon Zabler[c], Timm Weitkamp[a,d], Bernd R. Müller[b], Gerd Weidemann[b], Peter Modregger[a], John Banhart[e], Lukas Helfen[a], Andreas N. Danilewsky[f], Hans G. Gräber[g], Richard Heldele[a], Boaz Mayzel[h], Jürgen Goebbels[b], Tilo Baumbach[a]

[a]Forschungszentrum Karlsruhe GmbH / K.I.T., Postfach 3640, 76021 Karlsruhe, Germany;
[b]Federal Institute for Materials Research and Testing, Unter den Eichen 80, 12200 Berlin, Germany;
[c]Max-Planck Institute of Colloids and Interfaces, Golm, 14476 Potsdam, Germany;
[d]European Synchrotron Radiation Facility, BP 220, 38043 Grenoble, France;
[e]Hahn-Meitner Institute/Helmholtz Centre Berlin; Glienickerstr. 100, 14109 Berlin,Germany;
[f]Albert-Ludwigs-University, Hermann-Herder-Str. 5; 79104 Freiburg, Germany;
[g]Rheinisch Westfälische Technische Hochschule, Pauwelsstr. 30, 52074 Aachen, Germany;
[h]Tel-Aviv University, PO Box 39040, Tel-Aviv 69978, Israel

ABSTRACT

The BAM*line* at the BESSY light source in Berlin and the TopoTomo beamline at the ANKA synchrotron facility in Karlsruhe (both Germany) operate in the hard X-ray regime (above 6 keV) with similiar photon flux density. For typical imaging applications, a double multilayer monochromator or a filtered white beam is used. In order to optimise the field of view and the resolution of the available indirect pixel detectors, different optical systems have been installed, adapted, respectively, to a large field of view (macroscope) and to high spatial resolution (microscope). They can be combined with different camera systems, ranging from 16-bit dynamic range slow-scan CCDs to fast CMOS cameras. The spatial resolution can be brought substantially beyond the micrometer limit by using a Bragg magnifier. The moderate flux of both beamlines compared to other 3rd generation light sources is compensated by a dedicated scintillator concept. For selected applications, X-ray beam collimation has proven to be a reliable approach to increase the available photon flux density. Absorption contrast, phase contrast, holotomography and refraction-enhanced imaging are used depending on the application. Additionally, at the TopoTomo beamline digital white beam synchrotron topography is performed, using the digital X-ray pixel detectors installed.

Keywords: microtomography, non-destructive evaluation, coherent imaging, X-ray refraction, X-ray phase contrast, Synchrotron-CT, synchrotron instrumentation, scintillator, Bragg magnification, holotomography, X-ray topography

1. INTRODUCTION

During the 1990s, X-ray micro-imaging was established on various existing and at that time newly-built (third generation) synchrotron light sources, such as the European Synchrotron Radiation Facility (ESRF), the Advanced Photon Source (APS) or the Daresbury Synchrotron Radiation Source [1,2,3,4,5]. Furthermore, the ongoing detector developement allowed to reach submicrometer resolution by the end of that decade [6]. The outstanding image quality of X-ray radiographs and tomographs, acquired by using synchrotron radiation, in terms of resolution, contrast and low noise level led to numerous discoveries in fields like life sciences, materials research or paleontology. Subsequently, the increasing number of publications based on results achieved by synchrotron micro-imaging attracted more and more beamline users. This development is well documented since 1997 by the proceedings of this SPIE conference series "Developments in X-ray Tomography". Well-established imaging beamlines like ID15, ID19 (both ESRF), 2-BM (APS) or TOMCAT (SLS) receive several times more beamtime requests than can be granted, which shows the strong demand for synchrotron-based high resolution imaging stations [1,2,7,8,9].

In this article we describe the imaging instrumentation of the BAM*line* (located at the BESSY light source in Berlin)

*arack@snafu.de; phone +49 7247 82 6288; fax +49 7247 82 8677; www.fzk.de/anka

Developments in X-Ray Tomography VI, edited by Stuart R. Stock,
Proc. of SPIE Vol. 7078, 70780X, (2008) · 0277-786X/08/$18 · doi: 10.1117/12.793721

and the TopoTomo beamline at the ANKA facility in Karlsruhe, both in Germany. The two beamlines work with similar peak photon flux density values around 10^{11} ph/s/mm^2, assuming an energy bandwidth of around 1% as typically reached when employing multilayer monochromators. This moderate photon flux limits the performance compared to beamlines of other third generation light sources (with ring energies above 3 GeV), which offer a peak photon flux density of one or two orders of magnitude higher (assuming again the use of multilayer monochromators). Nonetheless, using an optimized detector concept, we established spatial resolution up to 2 µm for standard applications (effective pixel size < 1 µm). For selected applications, X-ray beam collimation has proven to be a reliable approach to increase the available photon flux density by up to one order of magnitude [10]. For other methods like fast phase contrast radiography on living species a white beam mode delivers the required higher photon flux density [11]. The spatial resolution of the imaging setups can be brought substantially beyond the micrometer limit by using a Bragg magnifier in one or two dimensions. Different contrast modes like absorption contrast, phase contrast, refraction enhanced contrast or holotomography are available as well. Both beamlines are dedicated to inhouse research and applications by external users.

2. BEAMLINE LAYOUTS

In Figure 1 the optical section of the BAM*line* is sketched. The synchrotron light coming from a superconducting 7T wavelength shifter source can be monochromatised via a fully automated double multilayer monochromator (DMM) and/or a double crystal monochromator (DCM). The multilayer structures of the DMM suppress the second harmonic; an energy bandwidth of 1.7 % was measured at 20 keV. Slit systems are available upstream of the DMM (aperture), downstream of the DCM and in front of the experimental station. The only vacuum window of the beamline is a differentially-pumped double Kapton foil located upstream of the experimental station. An in-vacuum absorption filter system consisting of different polished metal foils (Al, Be, Cu) is placed upstream of the DMM. It can be used to reduce the heat load on the first multilayer mirror and to suppress lower energy photons, which could otherwise pass the monochromator by means of total reflection and therefore deteriorate the monochromaticity. The downstream multilayer of the DMM can be bent to vertically (meridionally) focus the X-ray beam. The crystal monochromator allows horizontal (sagittal) focusing. Due to the available photon flux only the DMM is used for microimaging. The effective source size when using the DMM was measured by Talbot imaging to be 164 µm × 41 µm (horizontal × vertical, FWHM). The experimental station is located 37 m away from the source, which largely eliminates the influence of the finite source size on image quality [10,12,13].

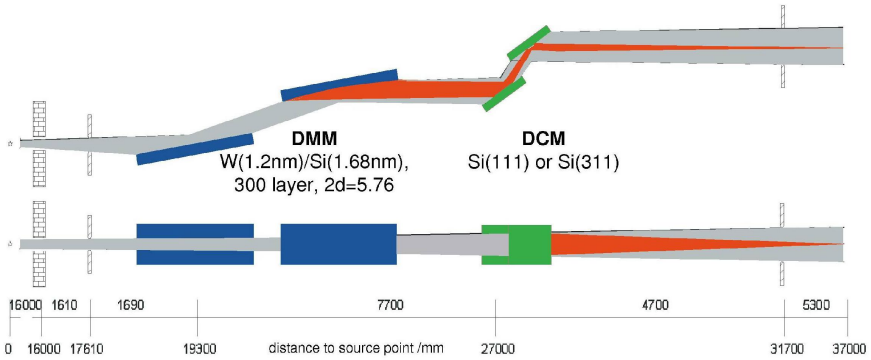

Fig. 1. Layout of the X-ray beam path at BAM*line* – BESSY (top: side view, bottom: top view). The radiation originating from a 7T superconducting wavelength shifter can be monochromatized using a double multilayer monochromator (DMM) and/or a double crystal monochromator (DCM), including a vertical focusing option for the DMM and a horizontal for the DCM [10,12,13]. The beamline can be run in white beam mode as well.

The layout of the TopoTomo beamline (as displayed in Figure 2) contains only one monochromator, a DMM (to be installed early 2009). TopoTomo is located at one of ANKA's bending magnet ports, dedicated since 2006 to direct and indirect imaging techniques. Similar to the BAM*line* design the DMM will contain a vertical focusing option. An absorption filter system is placed upstream of the DMM. In order to maximize the flux the monochromator will contain two multilayer stripes with different material composition (identical layer number and *d* spacing) which allows one to avoid absorption edges of the coating materials. Two in-vacuum slit systems are installed: one close to the source (aperture) and one upstream of the Be exit window. (Like the BAM*line*, TopoTomo has a single vacuum window located immediately upstream of the experimental station.) The source size of TopoTomo is 500 µm × 150 µm (horizontal × vertical FWHM). The primary slits are located 6 m from the source, which is close enough to efficiently use them for the

creation of a smaller secondary source for selected phase contrast applications that require spatial coherence in the horizontal plane[14]. The high-precision secondary slit system can be used to reduce the beam height at the sample position to approximately 10 µm for section topography [15]. The experimental station is placed 30 m away from the source. The installation of a DCM for TopoTomo is planned for a later upgrade of the beamline, e.g. to perform monochromatic topography or rocking curve imaging.

3. IMAGING STATIONS

3.1 Cameras

Different cameras are available in order to optimize detector performance, depending on the application. Microtomography typically requires a relatively high dynamic range, such as typically provided by back-illuminated slow-scan CCDs. Both at the BAM*line* and at TopoTomo, a PCO 4000 CCD-based camera (PCO AG, Kelheim, Germany) is used. Its dynamic range of 5.000 gray levels at a maximum readout speed of 2×8 MHz and the 4008×2672-pixel chip (9 µm pixel size) are perfectly suited for standard microtomography applications. Additionally, a fast read-out mode of 2×32 MHz is available. 4 GByte on-board memory allow for fast data acquisition rates[16]. For high performance applications the ESRF-developed FReLoN 2k14 CCD camera is available at TopoTomo[17], for low-flux applications at the BAM*line* the back-illuminated slow-scan CCD camera VersArray:2048 by Princeton Instruments[10]. High speed applications like fast microradiography are realized using standard CMOS cameras such as the PCO 1200.hs [18].

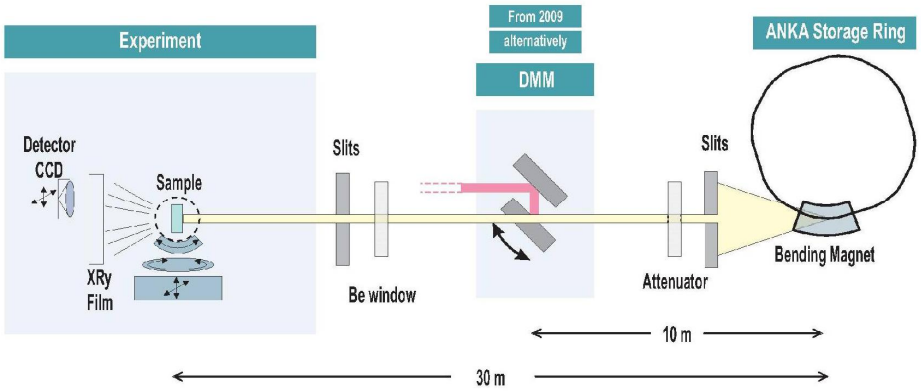

Fig. 2. Layout of the TopoTomo beamline at the ANKA light source [14]. The radiation originating from a 1.5-T bending magnet can be filtered by using different metal foils or silicon wafers. From 2009 on, a fixed-exit double multilayer monochromator will be available, with approx. 1.5% spectral bandwidth and a vertical focusing option. The beamline can be run in white beam mode as well.

3.2 Detector systems

Similar to the camera pool we use different X-ray-to-light converter and projection systems in order to be more flexible in optimizing the performance of our apparatus to the individual demands of the experiment. The principle design of our detectors follows the concepts of Bonse and Busch [5] and Koch et al.[6]: the luminescence image of a scintillating screen is coupled via visible light optics to a digital camera (Figure 3, left). We would like to remark that the first use of indirect X-ray pixel detectors was live X-ray topography performed in the 1970s by Hartmann et al.[19]. The best achievable resolution of these indirect detectors is the Abbe limit determined by the numerical aperture of the front objective (corrected by the refraction on the scintillator substrate) and the scintillator's wavelength of maximum emission. We use additional glass filters in the beam path of the visible light. They suppress parasitic scintillation (which can be emitted e.g. by the scintillator substrate) and block light which is beyond the chromatic corrections of the optics. Spectrally neutral density filters can be used to adapt the ratio of converted X-ray (scintillator) vs. detected luminescence photons (camera) in order to fully exploit the dynamic range of the digital camera and optimize the signal-to-noise ratio. A diaphragm (iris) in the optical beam path is applied in order to trim the numerical aperture to the effective pixel size of the detector system. For high resolution up to the sub-micrometer scale, we use a commercially available system (Optique Peter, Lyon, France) which uses Olympus microscope objectives in an adapted optical design developed originally in cooperation with the team of the ID22 beamline at ESRF [2] (Figure 3, right), and since then adopted by other instruments including the tomography instrument at SLS (Switzerland) and ESRF-ID19. For moderate resolutions we use Rodenstock objectives with a large numerical aperture in combination with a Nikon tele-objective Nikkor 180/2.8

ED (Figure 3, middle). This unique design allows us to work with large field of view / low magnifications between 1.5x and 9x while achieving a high visible light throughput [10]. Besides imaging of objects with a large field of view the system has also been proven to be perfectly suited for fast white beam radiography at ANKA's TopoTomo beamline, reaching imaging speed of up to 250 frames per second [11].

3.3 Scintillators

The efficiency of an indirect detecting system is driven by the stopping power of the material used as scintillating screen. Different aspects have to be taken into account when choosing the scintillator. First, the attenuation coefficient of a given scintillator material can change drastically with the X-ray photon energy, allowing an improvement of a factor of 2 by selecting the strongest stopping material. Second, due to the decreasing depth of focus of visible light optics with increasing magnification, thinner scintillators are required to obtain higher resolution. In practice, for the highest spatial resolutions, in the sub-micrometer range, the scintillator thickness should not exceed a few microns. But only a few scintillating materials have been successfully grown so far as thin films by liquid phase epitaxy techniques, e.g. LuAG:Eu, GGG:Eu or LSO:Tb [6,20,21]. Short exposure times for fast real-time imaging require short response times of the scintillator. We currently use 5-µm-thick LuAG:Eu crystals grown by liquid phase epitaxy on top of undoped YAG substrates (CEA LETI, Grenoble and FEE GmbH, Germany) for imaging with sub-micrometer resolution, LuAG:Eu with 10 or 25 µm thickness for resolutions between 1 µm and 2 µm. 40 µm thick CWO and BGO crystals are for resolutions around 4 µm, up to 300 µm thick CWO and LYSO:Ce large area crystals for moderate resolutions with a large field of view. Different LuAG:Ce crystals are currently under commissioning.

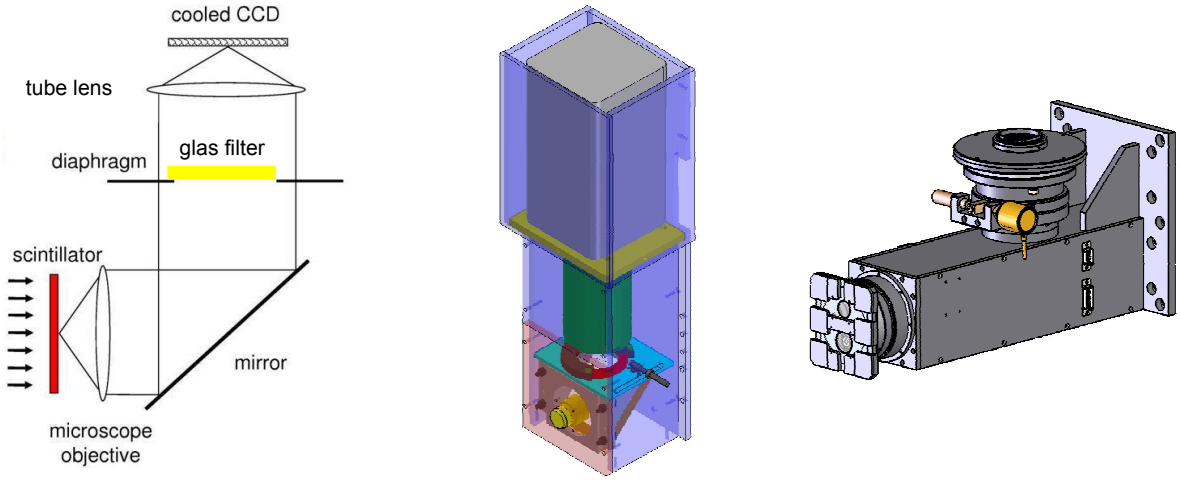

Fig. 3. Left: indirect detection concept using scintillators and microscope optic with a folded beam path for the visible light [5,6]. Middle: macroscope detector for large view fields view (BAM*line* design) [10]. Right: microscope for high resolution imaging (Optique Peter, Lyon).

Figure 4 demonstrates the resolving power of our high resolution detection system by showing radiographs of a commercially available X-ray test pattern (model X500-200-30, Xradia Inc., Concord, CA, USA). The left part of Figure 4 shows highest resolution achieved at TopoTomo in white beam mode when combining a 4 µm thin LuAG:Eu single crystal with a Olympus 20x objective (NA 0.75, 0.2 µm effective pixel size). Figure 4 (right) shows a selected region of the test pattern imaged at the BAM*line* with a collimated and a non-collimated synchrotron beam with a spatial resolution < 2 µm (0.7 µm effective pixel size). No change in resolution can be seen when the distance sample to detector is kept small (5 mm in our case).

3.4 Analyzer-based imaging & Bragg magnification

Analyzer-based imaging (ABI) is performed at the BAM*line* in order investigate the changes and development of inner surfaces of high performance composites, ceramics and other advanced materials, which show anisotropy, heterogeneity and complex shapes [10,22]. The X-ray refraction reveals the inner surfaces and interfaces, allowing us to determine particles with sub-micrometer size, cracks and pore sizes. To perform the measurement, a parallel monochromatic beam (up to 60 keV) from the DMM (or the DCM) is used. As is well known, the rocking curve of a crystal pair is usually

recorded by tilting the second crystal against the first crystal around the Bragg angle while measuring the reflected intensity. For ABI, the highly collimated and monochromatized beam from the first crystal traverses a specimen placed between the two crystals and is attenuated due to the specimen's absorption properties. Additionally, X-rays are deflected at all interfaces in the sample due to refraction. This leads to a broadening of the rocking curve. As a consequence, all X-rays scattered at angles larger than the rocking curve width are stopped by the second crystal, if the crystal pair is set to the maximum of the rocking curve. The result is a significant contrast enhancement in the radiographic projection image of the sample. If the second crystal is slightly off the rocking curve maximum only the scattered X-rays will be reflected and detected by the camera. The same setup can be used in order to achieve a resolution of down to a few hundred nanometer by asymmetric Bragg reflections as a beam width magnifier in front of the detector system. The analyzer crystal (second crystal) is replaced by an asymmetrically-cut Bragg crystal with an appropriate asymmetry angle. A set of crystals provide a magnification of a factor of 20 at 10 keV, 20 keV, 30 keV and 40 keV photon energy, respectively. The axis of rotation of the specimen can be aligned perpendicular or parallel to the scattering plane of the crystal, to define the orientation of the magnification plane in the reconstruction.

A so-called *Bragg magnifier* for TopoTomo is currently under commissioning. The system consists of two analyzer crystals with perpendicular diffraction planes in order to provide two-dimensional magnification. Spatial resolution of 0.4 µm was experimentally demonstrated [23], while the angular sensitivity, which is directly related to the sensitivity of density variations present in the sample, has been theoretically estimated to be in the order of micro-radians [24]. In order to increase the photon flux density, an adapted double crystal monochromator (DCM) with asymmetric Bragg reflections for beam compression will be installed locally together with the Bragg magnifier. Since the field of view of the Bragg Magnifier is 2 *x* 2 mm^2 at maximum, it is preferable to use a horizontal monochromator setup because the beam can be compressed more strongly due to the larger horizontal beam size. A compression factor of 7 is planned for the entire DCM resulting in a gain of flux density in the same order.

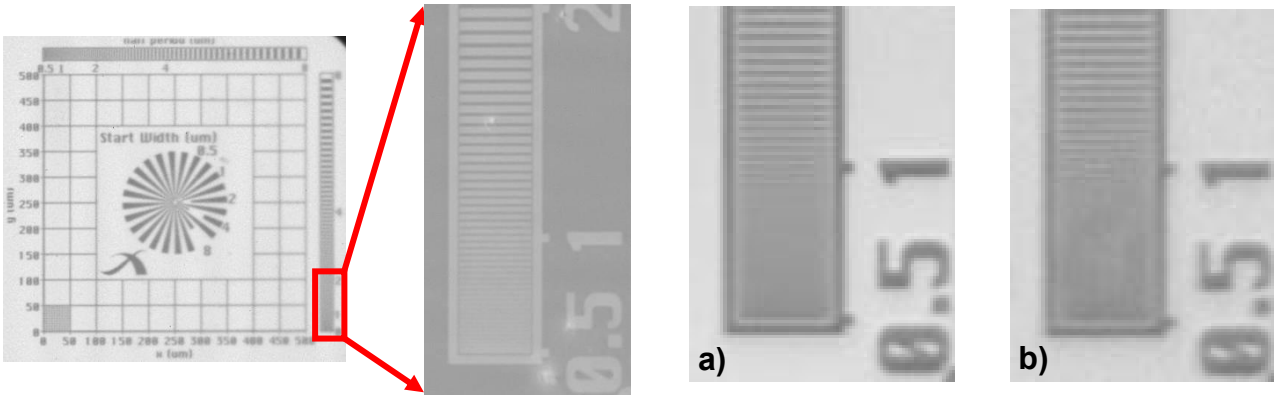

Fig. 4. Left: Xradia test pattern (X500-200-30), a selected region was imaged using a Olympus 20x objective (0.75 NA) in combination with a 4 µm thick LuAG:Eu scintillator in white beam mode at TopoTomo. Right (a): image of line pairs taken at the BAM*line* with a resolution < 2 µm (0.7 µm effective pixel size) and a maximal vertical collimated beam, (b): same section imaged with a non- collimated beam, no change in resolution is detectable (5 mm distance sample to detector) [10].

4. APPLICATIONS

Various experiments have been successfully carried out at the BAM*line* and TopoTomo beamline in recent years, e.g. microtomography on different samples from materials research [25,26,27,28], fast white beam phase contrast micro-radiography on living insects [11], micro-radiography and holotomography with subsequent image analysis on semi-solid alloys [29], digital white beam topography on 300 mm wafers [15,30]. Here we will present a few selected examples.

The first example is an investigation of demineralization processes in human teeth performed at the BAM*line*. High resolution synchrotron microtomography using monochromatic radiation has already proved to be perfectly suited for the quantification of mineralization density in tooth tissue [31,32]. As proof of concept we scanned a specimen taken from a human wisdom tooth which was immersed in water for 120 hours. The result is displayed in Figure 5 (left): the inset shows a 3D rendering of a sub-volume cut out of the tomographically reconstructed volume data. The line plot shows a

density profile along the direction of the red arrow (which indicates the surface as well). No change in mineralization can be seen. But after treating a similar sample for 120 h with a demineralizing liquid, the sample shows a significant density loss close to the surface, as can be seen in the right panel of Figure 5 (dark area in the volume rendering). The corresponding density plot reveals that in a region of approx. 150 µm depth beneath the surface, the density of the tissue was reduced by almost a factor of two. Additionally, hairline demineraization reaching deep into the enamel can be distinguished. Further investigations showed that a remineralisation process can be qualified by comparing microtomography scans of demineralized and remineralized samples [33].

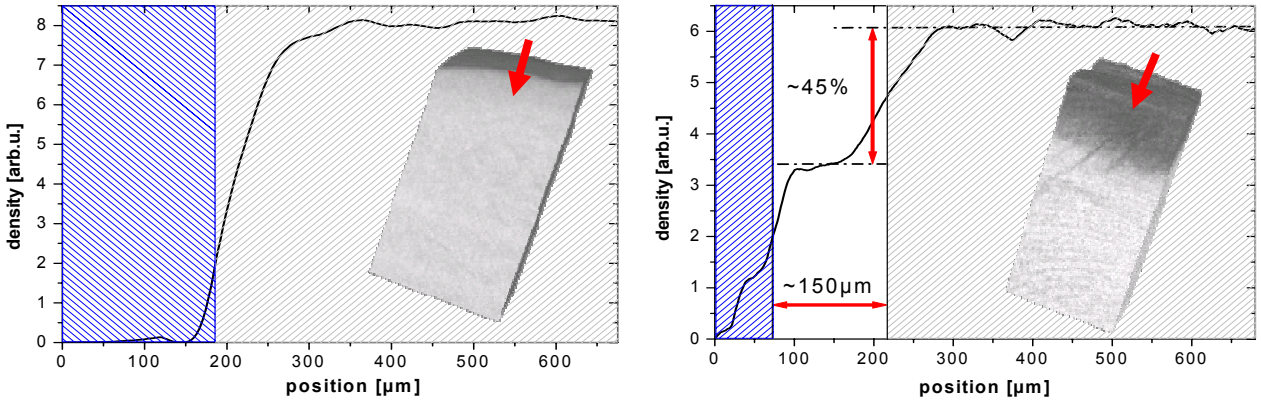

Fig. 5. Left: Density profile at the surface of human tooth tissue treated 120 h with water (blue: air, white: tooth tissue). The inset shows the investigated volume, the red arrow indicates the orientation of the depth profile relative to the surface. No demineralization distinguishable. Right: density profile at the surface of human tooth tissue treated 120 h with a demineralizing liquid. A strong loss of mineralization can be seen, also visible in the 3D rendering of the analyzed volume (inset) as dark area [33].

For TopoTomo we show investigations on skeleton parts of marine organisms. In detail, we look at spicules forming the silica skeleton of marine sponges. In this way we hope to resolve a number of questions, e.g. the possibility of a spiral structure of the core with a characteristic "pitch". This could be a species specific structure or specific to a certain spicule type that may be found in a number of different sponge species. The skeleton gives the sponge its shape and general body plan. It also allows it to endure forces such as currents and waves [34]. By reducing the source size to 150 µm *x* 150 µm via TopoTomo's aperture slit system we can visualize the core of a spicule by means of white beam phase contrast imaging. Figure 6 (left, a) shows a SEM image of a spicule core, Figure 6 (left, b) a tomographic slice of a comparable sample. These tomographic images of the spicule's core allow for a characterization of its shape and size throughout the whole spicule. This will enable us to create a three-dimensional model of the spicule showing structural layers and internal as well as external details.

A final example of tomographic investigations at TopoTomo for materials science applications is shown in Figure 6 (right). The tomographic slice shows an injection moulded green metallic micro part consisting of steel powder (6.5 µm mean particle size diameter, 63 vol-% powder loading). The aim of this study is to understand powder binder separations, a well known phenomenon in powder injection moulding (PIM). Due to the high surface to volume ratio in MicroPIM surface effects and also separation effects get more and more dominant. Synchrotron micro-tomography and subsequent image analysis were used to measure local particle size distributions and local particle densities in samples produced by MicroPIM [25].

5. SUMMARY & OUTLOOK

In this article we introduced the high resolution imaging stations at the BAM*line* (BESSY light source, Germany) and TopoTomo (ANKA light source, Germany). Both imaging facilities work with an instrumentation pool consisting of several cameras, optics, scintillators and mechanical stages. In combination with the flexible layout of the beamlines this allows one to optimize the imaging stations for different applications in terms of resolution, contrast modalities or image acquisition speed. The broad range of applications already performed at both beamlines with the subsequent peer-reviewed publications underlines that our instrumentation concept overcomes most of the limitations set by the moderate photon flux density available at both beamlines.

At the ANKA light source a dedicated insertion device beamline *IMAGE* is currently in the specification process. The beamline will be approximately 45 m long, fed by a super-conducting insertion device source (ANKA inhouse development) and house experimental stations for direct and indirect imaging techniques. Further imaging activities at ANKA which were not mentioned in this article are synchrotron computed laminography for imaging flat extended samples [35], the development and production of refractive lenses fabricated by deep synchrotron radiation lithography and fluorescence imaging [36,37].

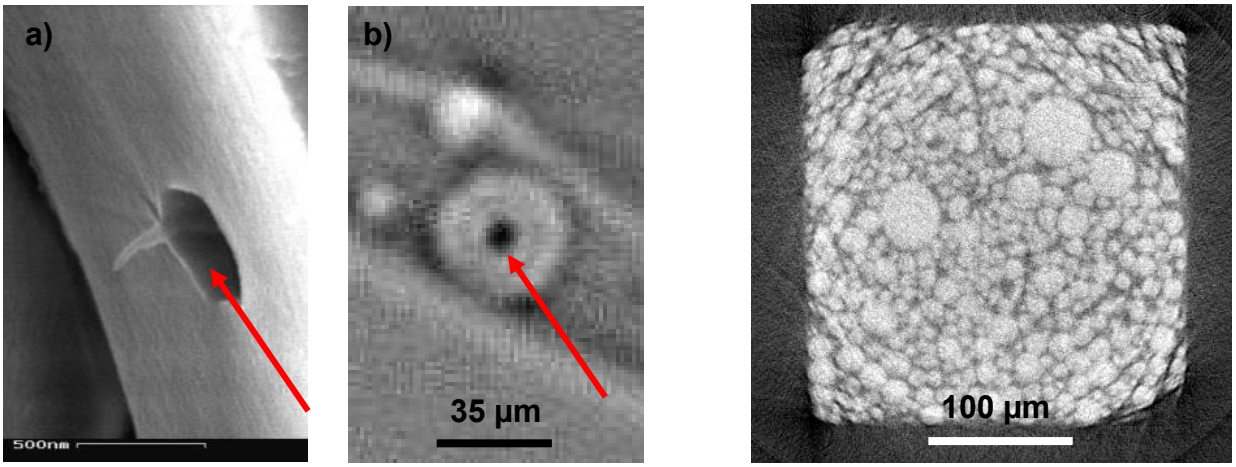

Fig. 6. Left: a) Scanning electron micrograph of a core of a sponge's spicule, b) tomographic slice of a comparable sample (0.9 µm pixel size, approx. 2.5 µm detector resolution). Right: tomographic slice of a sample produced by micro powder injection moulding. Steel powder with a mean particle size diameter of 6.5 µm and a powder loading of 63 vol-%. Acquired using TopoTomo's white beam mode, spatial resolution of the detector system is around 2.5 µm (0.9 µm effective pixel size).

ACKNOWLEDGMENTS

We acknowledge T. Spangenberg, W. Mexner, H. Schade, R. Lang, V. Heger, R. Stricker, H. Heinzmann, R. Kleinschmidt, W. Möck, C. Frieh, K. Abel, D. Erbe, U. Herberger, M. Cholewa, P. Vagovic, D. Pelliccia, A. Völcker, T. Fischböck, A. Cecilia, T. dos Santos Rolo, D. Haas, H. Waitz, A. Schult, J. König, C. Schulz (FZK) for the countless support, help, inspirations and discussions, M. Klinger, T. Wolk (BAM), M. Bruno (KPE GmbH) for constructions and technical support, C. Maucher (Micos GmbH) for support with high precision stages, K. Dupré (FEE GmbH) for help with all the single crystals, C. Rau (Diamond), M. Stampanoni (SLS), P. Zaslansky (MPG), F. De Carlo (APS) for all the inspirations and fruitful discussions, W. Tutsch (PCO) for support with PCO cameras, A. Homs Puron, V. Rey Bakaikoa, J.-C. Labiche (ESRF) for support of the FReLoN. Special thanks to Tanja.

This conference contribution was funded by the German Research Foundation DFG (KON 804/2008).

REFERENCES

[1] Cloetens, P., Ludwig, W., Baruchel, J., Van Dyck, D., and Van Landuyt, J., Guigay, J. P., Schlenker, M., "Holotomography: Quantitative phase tomography with micrometer resolution using hard synchrotron radiation X-rays", Appl. Phys. Lett. 75, 2912-2914 (1999).

[2] Weitkamp, T., Raven, C., Snigirev, A. A., "Imaging and microtomography facility at the ESRF beamline ID 22", Proc. of SPIE Vol. 3722, 311-317 (1999).

[3] Lee, H.-R., Lai, B., Yun, W., Mancini, D. C., Cai, Z., "X-ray Microtomography as a Fast Three-Dimensional Imaging Technology Using a CCD Camera Coupled with a CdWO4 Single-Crystal Scintillator", Proc. of SPIE Vol. 3149, 257-264 (1997).

[4] Hall, C., Barnes, P., Cockcroft, J. K., Colston, S. L., Haeusermann, D., Jacques, S. D. M., Jupe, A. C., Kunz, M., "Synchrotron energy-dispersive X-ray diffraction tomography", Nucl Instr Meth Phys Res A 140, 253-257 (1998).
[5] Bonse, U., Busch, F., "X-ray computed microtomography (μCT) using synchrotron radiation (SR)", Prog. Biophys. Molec. Biol. 65, 133-169 (1996).
[6] Koch, A., Raven, C., Spanne, P. and Snigirev, A., "X-ray imaging with submicrometer resolution employing transparent luminescent screens", J. Opt. Soc. Am., 15 (7), 1940-1951 (1998).
[7] Wang, Y., De Carlo, F., Mancini, D. C., McNulty, I., Tieman, B., Bresnahan, J., Foster, I., Insley, J., Lange, P., von Laszewski, G., Kesselmann, C., Su, M.-H., Thibaux, M., "A high-throughput x-ray microtomography system at the Advanced Photon Source", Rev. Sci. Instr. 72 (4), 2062-2068 (2001).
[8] Stampanoni, M., Groso, A., Isenegger, A., Mikuljan,G., Chen, Q., Meister, D., Lange, M., Betemps, R., Henein, S., Abela, R., "TOMCAT: A beamline for TOmographic Microscopy and Coherent rAdiology experiments", AIP Conf. Proc. 879, 848 (2007).
[9] Di Michiel, M., Merino, J. M., Fernandez-Carreiras, D., Buslaps, T., Honkimäki, V., Falus, P., Martins, T., Svensson, O., "Fast microtomography using high energy synchrotron radiation", Rev. Sci. Instrum. 76, 043702 (2005).
[10] Rack, A., Zabler, S., Müller, B. R., Riesemeier, H., Weidemann, G., Lange, A., Goebbels, J., Hentschel, M., Görner, W., "High resolution synchrotron-based radiography and tomography using hard X-rays at the BAMline (BESSY II)", Nucl Instr Meth Phys Res A 586, 327-344 (2008).
[11] Schmitt, C., Rack, A., Körner, L., Dieterich, A., Zabler, S., Betz, O., "High-speed X-ray cineradiography for imaging the mouthpart kinematics of living insects", ANKA Higlights (2008).
[12] Görner, W., Hentschel, M. P., Müller, B. R., Riesemeier, H., Krumrey, M., Ulm, G., Diete, W., Klein, U., Frahm, R., "BAMline: the first hard X-ray beamline at BESSY II", Nucl. Instr. Meth. A, vol. 467, 703-706 (2001).
[13] Riesemeier, H., Ecker, K., Görner, W., Müller, B. R., Radtke, M., Krumrey, M., "Layout and first XRF Applications of the BAMline at BESSY II", X-Ray Spectrometry 34, 160-163 (2005).
[14] ANKA Instrumentation Book, http://www.fzk.de/anka (2008).
[15] Danilewsky, A. N., Rack, A., Wittge, J., Weitkamp, T., Simon, R., Riesemeier, H., Baumbach, T., "White Beam Synchrotron Topography Using a High Resolution Digital X-ray Imaging Detector", Nucl. Instr. Meth. B, vol. 266, 2035-2040 (2008).
[16] pco.4000 - cooled digital 14bit CCD camera system, PCO AG / The Cooke Cooperation - http://www.pco.de .
[17] Labiche, J.-C., Mathon, O., Pascarelli, S., Newton, M. A., Ferre, G. G., Curfs, C., Vaughan, G., Homs, A., Carreiras, D. F., "The fast readout low noise camera as a versatile x-ray detector for time resolved dispersive extended x-ray absorption fine structure and diffraction studies of dynamic problems in materials science, chemistry, and catalysis", Rev. Sci. Instr. 78, 0901301 (2007).
[18] García-Moreno, F., Rack, A., Helfen, L., Baumbach, T., Zabler, S., Babcsán, N., Banhart, J., Martin, T., Ponchut, C., Di Michiel, M., "Fast processes in liquid metal foams investigated by high-speed synchrotron x-ray microradioscopy", Appl. Phys. Lett. 92, 134104 (2008).
[19] Hartmann, W., Markewitz, G., Rettenmaier, U., Queisser, H. J., "High resolution direct-display x-ray topography", Appl. Phys. Lett. 27 (5), 308-309 (1975).
[20] Martin, T., Koch, A., "Recent developments in X-ray imaging with micrometer spatial resolution", J. Synchrotron Rad. 13, 180-194 (2006).
[21] Dupré, K., Couchaud, M., Martin, T., Rack, A., "Szintillatorelement sowie Festkörperstrahlungsdetektor mit solchem", German Patent Application No. 10 2007 054 700.7 (2008), see as well http://www.scintax.eu .
[22] Müller, B. R., Lange, A., Harwardt, M., Hentschel, M. P., Illerhaus, B., Goebbels, J., Bamberg, J., Heutling, F., "First Refraction Enhanced 3D Computed Tomography", in: Proc. of the International Symposium on Computed Tomography and Image Processing for Industrial Radiology, ed. J. Goebbels, U. Zscherpel, DGZfP Proceedings BB 84-CD, ISBN 3-931381-48-X (2003).
[23] Modregger, P., Lübbert, D., Schäfer, P., Köhler, R., "Spatial resolution in Bragg-magnified X-ray images as determined by Fourier analysis", phys. stat. solidi (a) 204, 2746-2752 (2007).
[24] Modregger, P., Lübbert, D., Schäfer, P., Köhler, R., "Magnified x-ray phase imaging using asymmetric Bragg reflection: Experiment and theory", Phys. Rev. B 74, 054108 (2006).
[25] Heldele, R., Rath, S., Merz, L., Butzbach, R., Hagelstein, M., Haußelt, J., "X-ray tomography of powder injection moulded micro parts using synchrotron radiation", Nucl. Instr. Meth. B, vol. 246, 211-216 (2006).

[26] Rack, A., Zabler, S., Riesemeier, H., Weidemann, G., Müller, B. R., Helfen, L., Stiller, M., Knabe, C., Goebbels, J., Banhart, J., "Nondestructive 3D insights into foamy metals and bioregenerative ceramics", BESSY Highlights 2007, 34-35 (2008).
[27] Stiller, M., Rack, A., Dalügge, O., Zabler, S., Goebbels, J., Knabe, C., "Quantification of bone tissue regeneration employing β-tricalcium phosphate by three-dimensional non-invasive synchrotron microtomography – a comparative examination with histomorphometry", BONE (submitted 2008).
[28] Manke, I., Banhart, J., Haibel, A., Rack, A., Zabler, S., Kardjilov, N., Hilger, A., Melzer, A., Riesemeier, H., "In situ investigation of the discharge of alkaline Zn–MnO2 batteries with synchrotron x-ray and neutron tomographies", Appl. Phys. Lett., vol. 90 (20), article no. 214102 (2007).
[29] Zabler, S., Rueda, A., Rack, A., Riesemeier, H., Zaslansky, P., Manke, I., Garcia-Moreno, F., Banhart, J., "Coarsening of grain refined semi-solid Al-Ge32 alloy: X-ray micotomography and in-situ radiography", Acta Mat., vol. 55, 5045–5055 (2007).
[30] Danilewsky, A. N., Wittge, J., Rack, A., Weitkamp, T., Simon, R., McNally, P., "White Beam Topography of 300 mm Si-Wafers", J. Mater. Sci.: Mater. Electron. *in print* (2008). DOI 10.1007/s10854-007-9480-5
[31] Dowker, S. E. P., Elliott, J. C., Davis, G. R., Wilson, R. M., Cloetens, P., "Synchrotron X-Ray Microtomographic Investigation of Mineral Concentrations at Micrometre Scale in Sound and Carious Enamel", Caries Res. 38, 514-522 (2004).
[32] Kinney, J. H., Marshall Jr., G. W., Marshall, S. J., Hohling, H.-J., Wiesmann, U. P., Arends, J., Nelson, D. G. A., Malmqvist, K., Pashley, D. H., Schofield, R. M. S., "Three-dimensional mapping of mineral densities in carious dentin: Theory and method", Scanning Microscopy 8 (2), 197-205 (1994).
[33] Rack, A., "Untersuchung komplexer Materialsysteme mittels Synchrotron-Tomographie und 3D-Bildanalyse", Technical University Berlin, http://opus.kobv.de/tuberlin/volltexte/2006/1370/ (2006).
[34] Uriz, M. J., Turon, X., Becerro, M. A., Agell, G., "Siliceous spicules and skeleton frameworks in sponges: Origin, diversity, ultrastructural patterns, and biological functions", Microscopy Research and Technique 62 (4), 279-299 (2003).
[35] Helfen, L., Baumbach, T., Mikulík, P., "High-resolution three-dimensional imaging of flat objects by synchrotron-radiation computed laminography", Appl. Phys. Lett. 90 (7), 071915 (2005).
[36] Nazmov, V., Reznikova, E., Boerner, M., Mohr, J., Saile, V., Snigirev, A., Snigireva, I., Di Michiel, M., Drakopoulos, M., Simon, R., Grigorie, M. "Refractive lenses fabricated by deep SR lithography and LIGA technology for X-ray energies from 1 keV to 1 MeV", AIP Conference Proceedings (SRI2004) 705, 752-755 (2004).
[37] Simon, R., Buth, G., Hagelstein, M., "The X-ray fluorescence facility at ANKA, Karlsruhe: Minimum detection limits and micro probe capabilities", Nucl. Instr. & Meth. Phys. Res. B 199, 554-558 (2003).